Dissociation of cyclopropane in double ionization continuum

Oghbaie, Shabnam; Gisselbrecht, Mathieu; Månsson, Erik; Laksman, Joakim; Strahlman, Christian; Sankari, Anna; Ristinmaa Sörensen, Stacey

Published in:
Physical chemistry chemical physics : PCCP

DOI:
10.1039/C7CP01667K

2017

Document Version:
Early version, also known as pre-print

Journal Name

ARTICLE TYPE

Cite this: DOI: 10.1039/xxxxxxxxxx

Dissociation of Cyclopropane in Double Ionization Continuum†

Shabnam Oghbaie,*[a] Matheiu Gisselbrecht,[a] Joakim Laksman,[b] Christian Stråhlman,[b‡] Erik. P. Månsson,[b‡] Anna Sankari,[a] and Stacey L. Sorensen[a]

Received Date
Accepted Date

DOI: 10.1039/xxxxxxxxxx

www.rsc.org/journalname

Dissociative double photoionization of cyclopropane using tunable synchrotron radiation has been studied with an ion-ion coincidence time of flight experiment. With the aid of *ab initio* quantum calculations dication states and their favoured fragmentation pathways are determined, and compared with the experimental appearance energy and kinetic energy released of dissociation. State- (or bond)-selective dissociation in the ionization energy range of 25-35 eV have been investigated. Comparison of the measurement and calculation results, it is indicated that cyclopropane ring-deformation selectively triggered by tuning the photon energy, and the initially triggered ring-deformation effectively determines population of dication states working as a gateway for subsequent dissociation channels. At photon energies below the vertical double ionization threshold kinetic energy released of dissociation channels evidence sequential double ionization processes bridged via cyclopropane ring-opening populate Jahn-Teller components of $3e'^{-2}$ dication states, while analyzing the kinetic energy released of dissociation channels appearing above the vertical double ionization threshold evidence double ionization processes occurs predominantly at the Franck-Condon region populating $3e'^{-1}1e''^{-1}$ excited dication states.

1 Introduction

Controlling molecular fragmentation is one of the most active topics in photochemistry. Manipulating the outcome of molecular fragmentation requires knowledge about the underlying connections between electronic and nuclear dynamics. Cyclopropane is an ideal example to probe this connection. Due to the highly strained triangular carbon structure of the equilibrium geometry of D_{3h} symmetry significant ring deformation is induced following electronic transitions[1–3]. Bonding characteristics of cyclopropane have been studied extensively by means of photoelectron spectroscopy[2–6]. Intensive ring-deformation has been indicated on ionization spectrum of cyclopropane, where Jahn-Teller (J-T) distorsion of the orbitally degenerate $3e'^{-1}$ cation ground states leads to a doublet-structure[2,3]. Several theoretical studies aimed to understand these dynamics[7–10]. The potential energy surface of the $3e'^{-1}$ radical ion has been calculated with a saddle point at the equilibrium geometry and two global minima points with the two geometries of C_{2v} symmetry as shown in Fig. 1; one is characterized by a single elongated and two shortened C-C bonds (right side), and another one by two elongated and one shortened C-C bond (left side). From time-dependent point of view, an instantaneous ring-deformation occurs with ionization of a $3e'$ electron reduces the molecular Coulomb field and, as pointed out by Wannier[11], reduces the molecular ionization energy of the ground equilibrium geometry, the so-called adiabatic ionization.

In the present study, we investigate nuclear dynamics upon photo double ionization of cyclopropane. Double ionization of doubly degenerate $3e'$ orbitals induces strong ring-deformation in the dication states. In particular, two hole localization on one of the $3e'$ orbitals leading to orbitally degenerate dication states has implications on the Jahn-Teller interaction and the subsequent dissociation pathways. The strong electron nuclear correlation enhances sequential double ionization processes where ionization of two electrons are bridged by the nuclear motion coupled to the ionization. This means by measuring appearance energy (AE) and kinetic energy released (KER) of dissociation channels the photon energy sharing among the two electrons and the intervening nuclear motions are characterized. For this purpose, tunable synchrotron radiation combined with a 3-D ion momentum imaging technique is used to fully investigate dissociation dynamics of double ionization. Coincidence measurements of ion pairs upon energy-selective double ionization allows us to characterize the underlying connection between the electronic and nuclear dynamics. In particular, coincident ion fragments detected

[a] *Department of Synchrotron Radiation Research, Lund University, Lund S-221 00, Sweden; E-mail: shabnam.oghbaiee@sljus.lu.se*
[b] *Department of Cell and Molecular Biology, Uppsala University, Uppsala, Sweden*
[b†] *Institute for Photonics and Nanotechnologies, IFN-CNR, Milan, Italy*
[b‡] *MAXIV Laboratory, Lund University, Lund, Sweden*

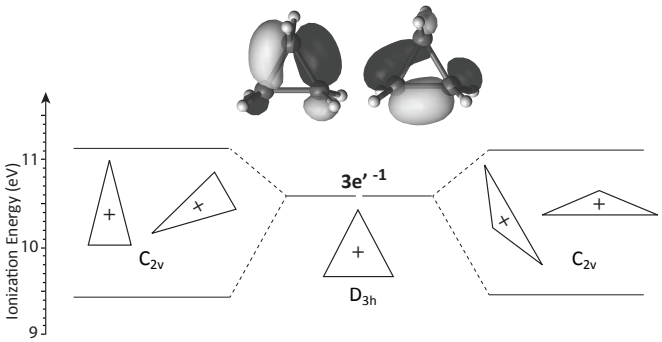

Fig. 1 The doubly-degenerate cyclopropane cation states ($3e'^{-1}$) in the D_{3h} symmetry undergo a Jahn-Teller splitting into a lower and higher components along distortion to the geometries of C_{2v} symmetry. Single ionization from each orbital leads to equally distortion along the ring-opening coordinates, either via one elongated (rigth side) or via two elongated (left side) C-C bonds. Site of the bond elongations is determined by the bonding character of the removed electron. The molecular orbitals were obtained using cc-pVDZ basis set and the self-consistent field (SCF) calculation. In this work, we investigate that to what extent the Jahn-Teller interaction contributes to the double ionization process of cyclopropane.

with photon energy below the vertical double ionization potential threshold (at fixed equilibrium geometry) indicate mechanisms of the instantaneous nuclear dynamics. The experimental results are combined with an *ab initio* quantum calculation to reveal the involved dication gateway states and their minimum reaction pathways towards the observed dissociation products.

2 Experimental method

The measurements were carried out on the 6.63 m off-plane Eagle normal-incidence monochromator at beam line I3 at the MAX III electron storage ring at MAX-laboratory in Lund, Sweden [12,13]. The light source is an Apple II undulator which was used in the linear polarisation configuration. The entrance and exit slits of the monochromator have been adjusted to give a photon band width <0.5 meV. In order to avoid spurious effects due to ionization by higher-order photons a magnesium film filter was placed in the synchrotron radiation beam.

We use a multiple-ion coincidence 3D-momentum imaging spectrometer to study fragmentation of molecules. Since a detailed description of the apparatus and data reduction techniques have been in course of publication previously [14,15], only a brief description will be given here. The spectrometer consists of a *Wiley McLaren Time Of Flight* (TOF) mass-spectrometer, equipped with a MCP-position sensitive detector *delay line anode* (DLD), and an electron detector. The energy selected synchrotron light beam crosses an effusive molecular beam in the extraction region so that electrons and ions are extracted from the center in opposite directions by a DC electric field. The ionized electron starts the acquisition time and the TOF spectrometer with two stages acceleration with an electrostatic lens launches all charged particles toward 80 mm diameter ion detector. At each photon energy fragment ions are identified on the TOF mass spectrum, after rescaling their time using $T \propto \sqrt{m/q}$. The AE of individual dissociative double ionization channels are determined using ion-ion coincidence measurements. The coincidence data is depicted on the ion-ion correlation map, where the x-axis represents the lighter mass fragments and the y-axis represents the heavier mass fragment. The temporal spread on each channel is also proportional to the total KER ($\Delta T \propto \sqrt{E_k}$).

Table 1 Electronic configuration, maximal coefficient, spin, and energy for the first 16 dication states of D_{3h} symmetry of cyclopropane (C_3H_6). The energy values are calibrated according to the energy of the equilibrium geometry of the neutral ground state. The dication excited states are made of 10 electrons in the $1a_2'' \; 3a_1' \; 1e'' \; 1e'' \; 3e' \; 3e'$ orbitals and 0 electron in the $2a_2'' \; 1a_2' \; 4e' \; 4e'$ orbitals. The occupation of orbitals in the active space is shown, where 2 implies doubly-occupied orbital, u and d imply singly-occupied orbital with electron spin up and down.

state	conf	coef	spin	energy [eV]
$\mathbf{3e'^{-2}}$	2222uu	0.98	T	31.28
	2222ud	0.76	S	32.16
	222220	0.65	S	32.59
	222202	0.63	S	32.59
$\mathbf{1e''^{-1}3e'^{-1}}$	22u22u	0.79	T	32.77
	22u22d	0.52	S	33.11
	222uu2	0.80	T	33.24
	22u2u2	0.68	T	33.24
	22u2d2	0.65	S	33.47
	222ud2	0.63	S	33.47
	222u2u	0.67	T	33.65
	222u2d	0.79	S	34.16
$\mathbf{1e''^{-2}}$	22uu22	0.96	T	34.51
	22ud22	0.80	S	35.29
	220222	0.79	S	36.16
	222022	0.78	S	36.16

3 Computational details

The equilibrium geometry of the neutral cyclopropane ground state of D_{3h} symmetry was optimized in the level of density functional theory (B3LYP) [16] using the 6-31G* basis set, and the vertical Double Ionization Potential (DIP_V) was obtained at 31.28 eV. To our knowledge the cyclopropane DIP_V has not been reported elsewhere; however, the calculated adiabatic double ionization potential (DIP_A) at 25.04 eV corresponding to the trimethylene geometry, as the dication equilibrium geometry, agrees with the previously studied heat of formation of the $C_3H_6^{2+}$ isomers [17,18].

To see from which orbitals electrons are removed in the double ionization and to connect nuclear geometry to charge localization, we performed electronic structure calculations of the molecular dications. The first sixteen singlet and triplet electronic states of the dication were calculated, shown in Table 1, at the level of paralell CASSCF/CASPT2 method and cc-pVTZ basis-set as implemented in the MOLCAS software program [19,20]. Minimum reaction pathways for the observed dissociation products were obtained, in which the highest potential barrier in dissociation pathway and energy difference between the barrier and ground state of final fragments are evaluated with the experimental AE and KER of dissociation products, by which dication gateway states of the dissociation channels are determined.

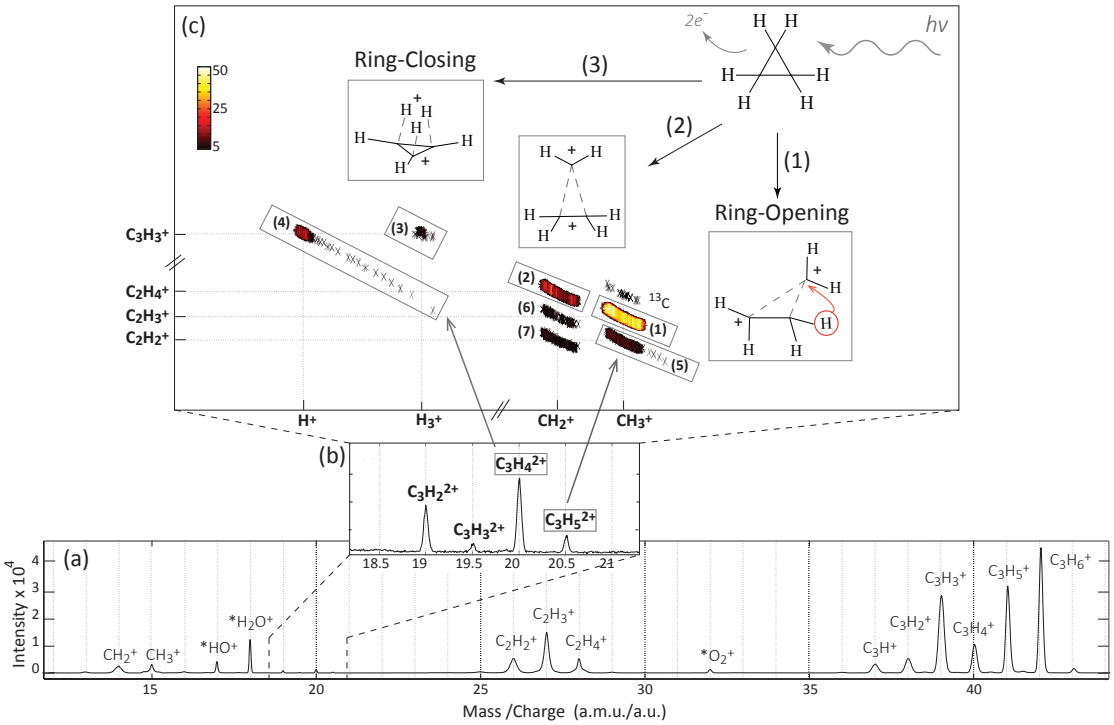

Fig. 2 Time of flight mass spectrum of cyclopropane at 35 eV photon energy (a). The zoomed-in region shows the doubly-ionized species $C_3H_{6-n}^{2+}$ ($n = 1-4$) stabilized by hydrogen evaporation (b). Ion-ion correlation map of the ion pairs at 35 eV photon energy (c). Channels are enumerated in order of the AE. An additional feature arising from the ^{13}C isotope is indicated in the figure. The required ring-deformations associated with the coincidences (1) (2) and (3) are shown schematically: ring-opening occurs differently on channels (1) and (2): by two unequal C-C bond elongation and by two equal C-C bond elongation, while ring-closing occurs on channel (3) by three simultaneous C-H bond elongations. Sequential dissociation pathways are indicated by the extended distribution at the end of channels (4) and (5), which are ascribable to delayed dissociation of the $C_3H_4^{2+}$ and $C_3H_5^{2+}$ specious.

4 Results and discussion

4.1 Dication states

Table 1 shows electronic energies of major configurations characterizing the first 16 singlet and triplet cyclopropane dication states. The first four dication states lying in the 31.28-32.59 eV energy region correspond to the double ionization of the doubly-degenerate $3e'$ orbitals. The ground dication state is a triplet state (uu) with 31.28 eV ionization energy where electrons of same spin are ionized from both of the doubly-degenerate $3e'$ orbitals (the two holes are delocalized in two orbitals). This transition is, in principle, spin-forbidden for direct double ionization. The second dication state has the same charge density but singlet multiplicity (ud) and 32.16 eV ionization energy. Double ionization from an identical $3e'$ orbital, where the two holes are localized in one orbital, leads to orbitally doubly-degenerate singlet dication states (*02-20*) with ionization energy of 32.59 eV. The next excited dication states lying in the 32.77-34.16 eV energy region correspond to the double ionization from $1e''$ and $3e'$ orbitals, and the four last excited dication states lying in the 34.51-36.16 eV energy region correspond to the double ionization of the doubly-degenerate $1e''$ orbitals.

4.2 Dissociative double ionization pathways

The measurements were carried out using tunable synchrotron radiation at a series of photon energies range from 25 to 35 eV in 0.5 eV steps. According to the calculated dication excited states, this energy region corresponds to about 6 eV below the DIP_V and population of the first 13 dication states. The TOF mass spectrum measured at 35 eV photon energy is shown in Fig. 2 (a). As can be seen in this figure, $CH_i^+ (i = 1-3)$, $C_2H_i^+ (i = 1-4)$, and $C_3H_i^+ (i = 1-6)$ are observed. The narrow peaks at m/z= 32, 18, and 17 marked with an asterisk are ascribable to O_2^+, H_2O^+, and OH^+ originating from the residual gas in the chamber. In addition to the peaks originating from single ionization, four peaks in the range from m/z=19 to 20.5 are also observed, these are the $C_3H_{6-n}^{2+}$ ($i = 1-4$) dictation species (shown in the zoomed-in region in Fig. 2 (b)). Dissociative double ionization leading to ion pairs are detected using ion-ion coincidence measurements. The ion-ion correlation color-map measured at 35 eV photon energy is shown in Fig. 2 (c). At this photon energy cyclopropane can dissociate into seven fragment ion pairs. Each coincidence represents a specific dication dissociation pathways. The appearance energy (AE) of the above dissociative double ionization channels are evaluated with the calculated cyclopropane dication states, as shown schematically in the energy diagram in Fig. 3. The dissociation channels in Fig. 2 (c) are enumerated in order of increasing AE.

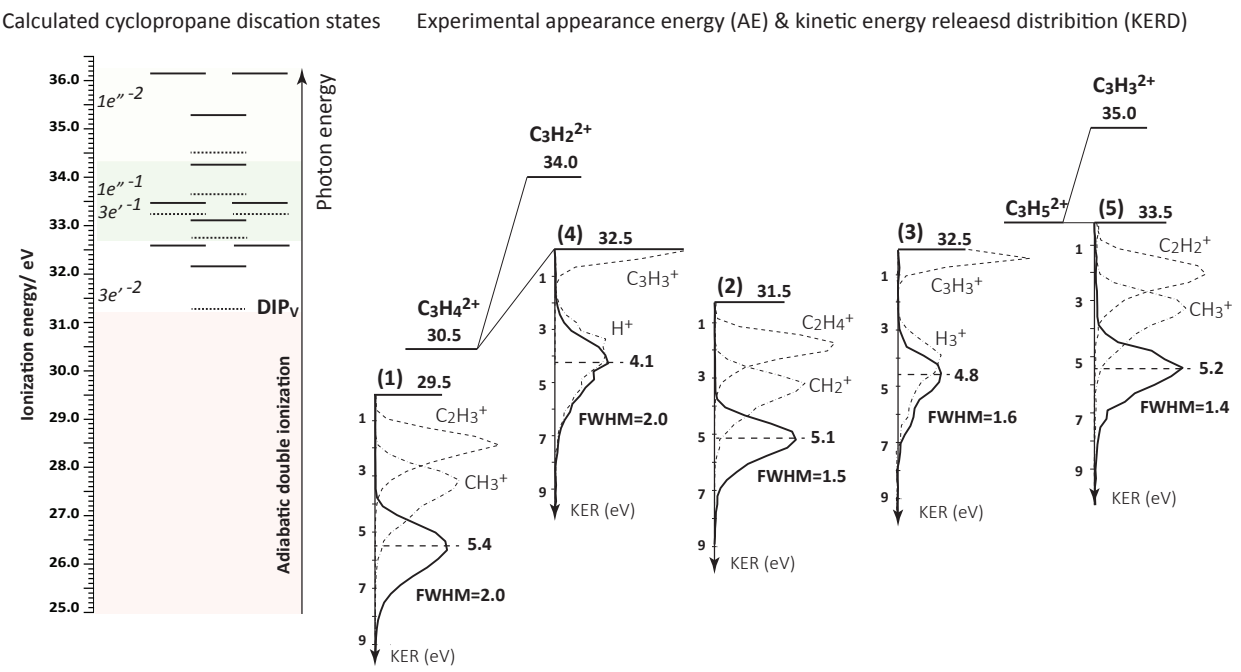

Fig. 3 Schematic representation of the calculated potential energy of cyclopropane dication states with the geometry of D_{3h} symmetry (on the left side), and experimental AE and KERD of the dissociation channels (on the right side).

It initially appears that two of the most intense dissociation channels are driven by double ionization of cyclopropane below the vertical threshold. The first channel in Fig. 2 (c) appears at 29.5 eV photon energy, about 2 eV below the DIP$_V$. This corresponds to dissociation into $CH_3^+/C_2H_3^+$ ion pair, where two C-C bond dissociation is required. Detection of the CH_3^+ ion in channel (1) is evidence of H-migration before C-C bond dissociation, as shown schematically in Fig. 2 (c). No parent dication $C_3H_6^{2+}$ is detected in the mass spectrum at m/z=21, but sharp peaks at m/z=20 corresponding to the $C_3H_4^{2+}$ dication are measured, indicating that two H-evaporation effectively stabilizes the dication species. In addition, the $C_3H_4^{2+}$ dication in Fig. 2 (b) appears at 30.5 eV photon energy, about 1 eV below the DIP$_V$. The intensive dissociation into channel (1) shows that the double ionization leaves the dication with sufficient internal energy for rapid dissociation into the $CH_3^+/C_2H_3^+$ ion pair; while the $C_3H_4^{2+}$ dication remains stable. The extended "tail" of the channel (4), $H^+/C_3H_3^+$ ion pair, in Fig. 2 (c) indicating delayed dissociation of the $C_3H_4^{2+}$ dication appears at 32.5 eV photon energy. The extended distribution, in fact, indicates that the $C_3H_4^{2+}$ dication is trapped behind a potential barrier, and slowly dissociates by tunneling. This process proceeds through the lowest potential barrier along two C-H bond dissociation into the $H^+/C_3H_3^+$ ion pair.

In the ion-ion correlation map of Fig. 2 (c) the first two appeared channels, (1) $CH_3^+/C_2H_3^+$ and (2) $CH_2^+/C_2H_4^+$, are both created through two C-C bonds elongation, however, as shown schematically in the figure, the ring-opening mechanisms underlying these channels differ; two unequally elongated C-C bonds favour H-migration in channel (1), while two equally elongated C-C bonds favour dissociation channel (2), the $CH_2^+/C_2H_4^+$ ion pair. Dissociation channel (2) appears at 31.5 eV corresponding to the energy region of $3e'^{-2}$ dication states [see Fig.3]. Increasing the photon energy to 32.5 eV, dissociation channel (3), the $H_3^+/C_3H_3^+$ ion pair, appears. Detection of the H_3^+ ion in this channel is evidence for simultaneous dissociation of three C-H bonds. Sequential dissociation of C-H bonds occurs at the same photon energy, producing channel (4). comparison of the intensity of channels (3) and (4) in the ion-ion correlation color-map of Fig. 2 (c), it appears that nuclear relaxation along ring-opening is preferred for driving dissociation channels, where avoiding ring-closing to produce H_3^+ ion. Increasing the photon energy to the energy region corresponding to the $3e'^{-1}1e''^{-1}$ dication states, at 33.0 eV, single hydrogen evaporation forms $C_3H_5^{2+}$ dication detected in the mass spectrum of Fig. 2 (b). An extended distribution in ion TOFs at the slightly end of the pathway (5) is seen in the ion-ion correlation map of Fig. 2 (c) where $CH_3^+/C_2H_2^+$ ion pair can indicate a delayed dissociation of $C_3H_5^{2+}$ dication. The appearance of the dissociation channel (5) at the same photon energy confirms that H-migration and dissociation into the $CH_3^+/C_2H_2^+$ ion pair occurs simultaneously after formation of $C_3H_5^{2+}$ dication. This explains the low intensity of $C_3H_5^{2+}$ peak compred to the $C_3H_4^{2+}$ peak in the mass spectrum of Fig. 2 (b). In addition to the above dissociation channels, further H-evaporation takes place at higher photon energies. As seen in the mass-spectrum of Fig. 2 (b), sharp peaks at m/z=20 and 19 corresponding to $C_3H_4^{2+}$ and $C_3H_2^{2+}$ specious are measured. These occur after evaporation of even numbers of hydrogens. Two small peaks at m/z= 20.5 and 19.5 corresponding to $C_3H_5^{2+}$ and $C_3H_3^{2+}$ specious are also observed after evaporation of odd numbers of hydrogens. The pattern in dications missing even and odd num-

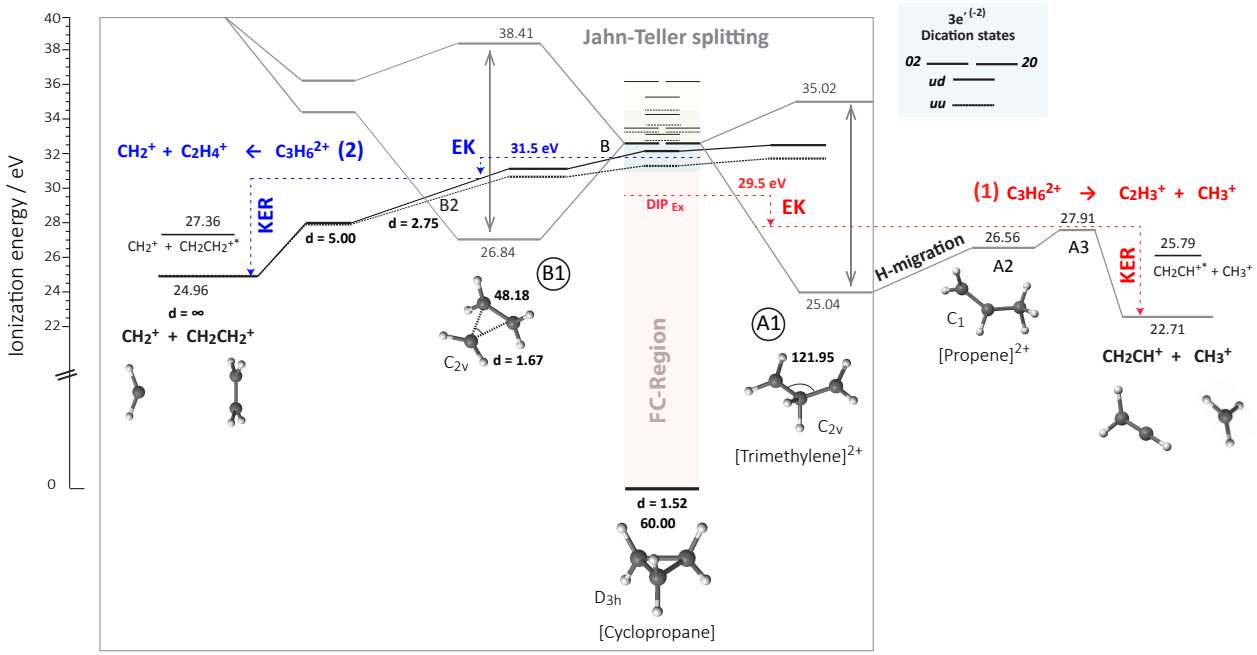

Fig. 4 Nuclear relaxation of the low-lying $3e'^{-2}$ dication states. The potential energy of the *uu/ud* states and the doubly degenerate 20/02 states in the Franck-Condon region of the D_{3h} symmetry are changes along the C-C bond coordinates. The Jahn-Teller (J-T) instability of the orbitally degenerate *20/02* states along the D_{3h} to C_{2v} ring-deformation symmetry breaking is shown in side the box. The favoured energy pathways for the dissociation channels (1) and (2) are calculated and compared with the experimental appearance energy (AE) and kinetic energy released (KER) of the dissociation, shown by the dashed-lines. The experimental double ionization potential DIP_{EX} is ascribed to the sequential double ionization process due to the strong coupling between $3e'$ ionization and C-C ring-deformation.

bers of hydrogen atoms suggests that two different pathways are feeding these channels.

The KER of dissociation into ion pairs seen in Fig. 2 (c) can be analyzed. The KERD of the dissociation channels (1) to (5) are shown in Fig. 3. Peak energies of the total KER distribution with the full width of the half maximum (FWHM) are indicated in the figure. These values are almost constant and independent to the ionizing photon energy, indicating that each dissociation channel take place in a specific internal energy region, from a certain gateway state to a certain fragment state.

4.3 Fragmentation driven by Jahn-Teller instability

The fact that several dissociation channels appear below the DIP_V implies that an instantaneous symmetry breaking takes place in the process of double ionization. To determine the shape of the involved potential energy surface, and correlate the dication states to the dissociation products, we performed a geometry optimization calculation on the low-lying $3e'^{-2}$ dication states. Due to the different bonding characteristics of the $3e'$ orbitals, nuclear dynamics of the *uu/ud* states differ from the *20/02* states: double ionization from one $3e'$ orbital (*20/02*) asymmetrically reduces the bonding character of C-C bonds over the ring-system, while double ionization from both $3e'$ orbitals (*uu/ud*) symmetrically reduces the bonding character of the C-C bonds over the ring-system. Accordingly, the potential energy of the $3e'^{-2}$ dication states varies differently along the C-C bond coordinate. As seen in Fig. 4, the Jahn-Teller (J-T) instability of the orbitally-degenerate *02/20* states in the equilateral triangle geometry of D_{3h} symmetry (Franck-Condon region) is reflected on the splitting of the potential energy along the C-C ring-deformation coordinates. Two optimized geometries of C_{2v} symmetry for the cyclopropane dication are calculated shown in Fig. 4: one by single elongated C-C bond into the (A1) geometry [trimethylene] with the CCC angle of 121.95^0 that lies at 25.04 eV energy region, and another one by two elongated C-C bonds into the (B1) geometry with the CCC angle of 40.185^0 that lies at 26.84 eV. For these geometries the lower J-T states lie below the DIP_V threshold (*uu/ud* states of D_{3h} symmetry). As was predicted based on the bonding characteristics of the $3e'$ molecular orbitals, the J-T instability of the *20/02* dication states is to a greater extent along the one elongated C-C bond (A1), and to a lesser extent along the two elongated C-C bonds (B1). The potential energy of the *uu/ud* dication states behave instead differently along the ring deformation coordinates; the potential energies slightly increase along the single elongated C-C bond and dramatically decrease along the double elongated C-C bond coordinates.

To address the question of to what extent ring-deformation intervenes double ionization of $3e'$ orbitals, we calculated minimum reaction pathways for the dissociation channels (1) and (2). The minimum energy dissociation pathway into the $CH_3^+/C_2H_3^+$ ion pair is shown on the right hand side of Fig. 4: the dissociation is driven by the J-T instability of the orbitally degenerate *20/02* states along the single elongated C-C bond, where in the lower J-T component the trimethylene dication (A1) rearranges into the propene isomer (A2) via a hydrogen atom migration. The propene dication dissociates into the CH_3^+/CH_2CH^+ ion pair

through the potential energy barrier of 27.91 eV (A3). Dissociation of the propene dication into the ground state of the fragments results in a KER of 5.2 eV. Comparing the experimental AE at 29.5 eV with the calculated potential barrier of dissociation at 27.91 eV, and comparing the experimental KERD of the dissociation peaked at 5.4 eV (FWHM=2.0 eV) [see Fig. 3] with the calculated KER of propene dissociation to the ground state of the fragments at 5.2 eV, it appears that ionization at 29.5 eV photon energy leaves 1.6 eV internal energy in the molecule not contributing to the dissociation, which in turn can be either associated to kinetic energy of autoionized electron in a sequential double ionization process or due to the dissociation into the internally (vibrationlly-electronically) excited final fragments. Considering the first excited state of the fragments lying at 25.79 eV, dissociation at 29.5 eV to the first excited state of fragments leads to the KER of dissociation at 3.71 eV, which is 1.7 eV below the experimental KER of dissociation. This indicates that a greater extent of the internal energy is decayed through autoionization in sequential double ionization process. The rapid dissociation at 29.5 eV potential energy region indicates that autoioniztion leaves the the lower Jahn-Teller component of the *20/02* states with sufficient internal energy to pass the potential barrier of propene dissociation, which in turn indicates the extent of nuclear motion preceded autoionization. We can speculate that the initially deposited internal energy to the highly excited singly ionized intermediate state is shared between coupled J-T active ring-opening nuclear motion and kinetic energy of $3e'$ ionization.

The minimum energy reaction pathway into the $CH_2^+/C_2H_4^+$ ion pair, channel (2), is shown on the left hand side of Fig. 4: equal elongation of two C-C bonds correlates the *uu/ud* dication states to the ground state of the $CH_2^+/C_2H_4^+$ ion pair. Although the potential energy of the *uu/ud* dication states decrease along this coordinate, the Jahn-Teller splitting of the *20/02* dication states decreases for the geometries where the length of two C-C bonds are longer than 1.67Å. This leads to conical intersections between the singlet *ud* state and the lower Jahn-Teller component at the two potential energies of 31.5 eV (B) and 28.55 eV (B2), where the length of two elongated C-C bonds are about 1.60 and 2.75 Å, respectively. The latter conical intersection (B2) provides a pathway for the lower Jahn-Teller component to dissociate into the ground state of the $CH_2^+/C_2H_4^+$ ion pair. The experimental AE of 31.5 eV indicates that, in fact, population of the *ud* (or *uu*) state is entirely essential for dissociation channel (2). Dissociation of the *ud/uu* states to the ground state of final fragments state leads to KER of 6.54 eV; however, the experimental KER of dissociation into the $CH_2^+/C_2H_4^+$ ion pair is peaked at 5.1 eV with FWHM of 1.5 eV. This indicate that dissociation at 31.5 eV photon energy leaves about 1.5 eV internal energy into the molecule, which in turn can either be associated to kinetic energy of autoionized electron in a sequential double ionization process or due to the internally excited final fragments. Considering dissociation at 31.5 eV to the first excited state of the fragments lying at 27.36 eV, this leads to KER of 4.14 eV which is 1 eV below the experimental value of KER. This can be interpreted by sequential double ionization that the internal energy of the highly exited singly ionized states is shared between kinetic energy of autoionization of $3e'$ electrons and ring-opening nuclear motion leading to population of the repulsive *uu/ud* dication states out of the Franck-Condon region. Regarding double ionization to the $3e'^{-2}$ gateway states, the relative ratio of dissociation channel (1) and (2) determines the extent of ring-opening intervening the double ionization processes: while highly excited singly-ionized intermediate states lying at 29.5 eV potential energy region mostly decay via elongation of one C-C bond to the lower component of the *20/02* states, the higher-lying intermediate states located above 31.5 eV potential energy mostly decay via elongation of two C-C bonds to the repulsive *ud/uu* states.

4.4 Ring-Opening vs. Ring-Closing

The experimental results [see Fig.3] show that increasing the photon energy above the DIP_V enhances the rate of C-H bond dissociation (H-evaporation). In order to confirm theoretically how efficiently the H-evaporation proceeds within doubly-charged cyclopropane, we calculated minimum reaction pathways for the channels involving C-H bond dissociation. The calculation results are depicted in Fig. 5. It is indicated that H-evaporation pathways can be sorted out based on whether the ring initially opens or closes: if H-evaporation is preceded by ring-opening along single elongated C-C bond coordinate, H_2-evaporation into formation of $C_3H_4^{2+}$ (A4) (allene) dication is preferred [see the right hand side of Fig. 5]; whereas when H-evaporation is preceded by ring-closing with three hydrogen atoms approaching each other [see the left hand side of fig. 5] the single H-evaporation into the $C_3H_5^{2+}$ (C2) dication is preferred. The calculation confirms that double ionization below the vertical threshold leaves the dication with sufficient internal energy for the molecular hydrogen evaporation into the $C_3H_4^{2+}$ (A4) dication [see the right hand side of Fig. 5], in which the ring-opening via single elongated C-C bond followed by H_2-evaporation from the middle carbon of trimethylene dication (A1), and creation of the allene dication (A4) with a molecular hydrogen at 27.92 eV ionization energy. The experimental AE of $C_3H_4^{2+}$ is, however, at 30.5 eV [see Fig.3] 1 eV below the DIP_V and 2.58 eV above the calculated energy of the ground state. According to the geometry calculation, single H-evaporation is associated with ring-closing [see the left hand side of fig. 5]. The minimum reaction pathway is obtained via the ring-closing dication (C1) that is followed by single H-evaporation and a hydrogen migration into the $C_3H_5^{2+}$ (C2) dication at 30.91 eV. The experimental AE of the $C_3H_5^{2+}$ dication is at 33.0 eV [see Fig.3] that is higher than DIP_V corresponding to the energy region of $3e'^{-1}1e''^{-1}$ dication states.

The creation of the $C_3H_4^{2+}$ and $C_3H_5^{2+}$ dication species is followed by further dissociation. In the ion-ion correlation map of Fig. 2 (c) the extended tail at the end of the dissociation channels (4) and (5) indicate delayed dissociation. The delayed dissociation of these dication species into the identical coincidences has been reported previously[21,22]. One photon double ionization of propane was reported a delayed dissociation of $C_3H_4^{2+}$ on a sub 100 ns time scale into the $H^+/C_3H_3^+$ ion pair[21]. One can speculate that ring-opening is followed by H_2-evaporation and delayed dissociation of the $C_3H_4^{2+}$ dication into the $H^+/C_3H_3^+$ ion pair:

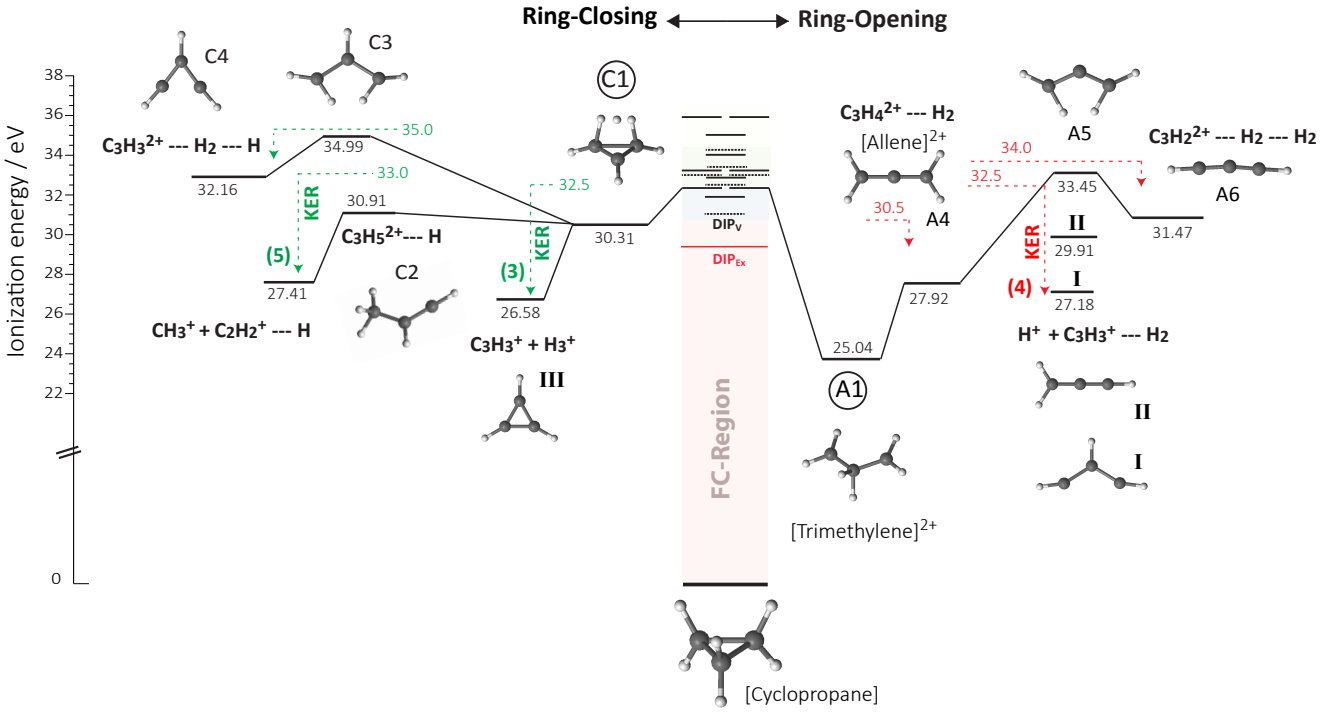

Fig. 5 The calculated minimum reaction pathways for H-evaporation indicates two group of pathways either triggered by ring-opening (A4)-(4)-(A6) or by ring-closing (3)-(C2)-(5)-(C4). The calculated values are compared with the experimental values of AE, indicated by the dashed-lines.

$C_3H_6 + h\nu \longrightarrow C_3H_6^{2+} + 2e^- \xrightarrow{(A4)} H_2 + C_3H_4^{2+} \xrightarrow{(4)} C_3H_3^+ + H^+$.
The experimental AE of 32.5 eV is indicated by the red dashed-line on the right hand side of Fig. 5. Experimentally, the ion pair is observed at the photon energy that is 2 eV above the AE of the $C_3H_4^{2+}$ dication. This means that the long-lived $C_3H_4^{2+}$ dication is created and trapped behind a potential barrier, and the trapping time is sufficient to allow molecular isomerization. Isomerization of $C_3H_4^{2+}$ dication via H-migration opens up dissociation channels via different final states, as is shown in the Fig. 5. This leads to different values in the KER of dissociation channel (4): C-H dissociation in the allene dication into the $H^+/C_3H_3^+$ (I) ion pair releases 2.6 eV kinetic energy, while C-H dissociation of CH_2CHCH and CH_3CCH dication isomers into the $H^+/C_3H_3^+$ (II) ion pair releases 5.3 eV to the fragments. The broad distribution of the experimental channel (4) [see Fig. 3] peaked at 4.1 eV with FWHM of 2.0 eV is a fingerprint of the hydrogen migration processes. In the ion-ion correlation map in Fig. 2 (c), at 32.5 eV photon energy the weak dissociation channel (3) appears. The calculated minimum energy pathway shown on the left hand side of Fig. 5 suggests that this channel is triggered by ring-closing, where three hydrogen atoms approach each other, dication (C1), leading to dissociation into the $H_3^+/C_3H_3^+$ (III) ion pair. The calculated AE of 30.31 eV (C1) is, however, far below the experimental AE of 32.5 eV. Comparing the calculated KER of dissociation to the ground state of the fragments at 3.7 eV with the experimental KER of 4.8 eV with FWHM of 1.5 eV, it appears that an excess amount of internal energy is released as the kinetic energy of the fragments. This is another evidence that the population of the excited $3e'^{-1}1e''^{-1}$ dication states is essential for the ring-closing pathways. As seen in Fig. 3, increasing the photon energy to 33.0 eV the $C_3H_5^{2+}$ dication is visible, but it simultaneously undergoes a metastable dissociation into the $CH_3^+/C_2H_2^+$ ion pair, channel (5). Metastable dissociation of the $C_3H_5^{2+}$ dication by electron impact ionization of propane into the $CH_3^+/C_2H_2^+$ ion pair has been previously reported[22]:

$C_3H_6 + h\nu \longrightarrow C_3H_6^{2+} + 2e^- \xrightarrow{(C2)} H + C_3H_5^{2+} \xrightarrow{(5)} CH_3^+ + C_2H_2^+$ (5)

in which an average KER of 4.58 eV is reported using the reverse reaction, indicating that essentially all available internal energy in the reaction is partitioned into kinetic energy of the fragments. Comparing the experimental KER of the dissociation peaked at 5.2 eV with FWHM of 1.4 eV [see fig. 3] with the calculated value at 3.51 eV, it is confirmed that the excess amount of internal energy following ionization at 33.0 eV photon energy is released to the fragments kinetic energy. The results specify that the excited $C_3H_5^{2+}$ dication associated with ring-closing is created in the energy region of the $3e'^{-1}1e''^{-1}$ cyclopropane dication states.

Increasing the photon energy above 33.0 eV leads to more extensive molecular rearrangements. According to the calculated minimum reaction pathways, the $C_3H_4^{2+}$ (A4) dication possesses a potential barrier at 33.45 eV for a CCC bending motion, where the two end-hydrogen atoms form a molecular hydrogen and $[CHCCH]^{2+}$ (A6) dication. The experimental AE of 34.0 eV for the $C_3H_2^{2+}$ dication in the mass spectrum of Fig. 2 (b) agrees well with the calculated potential barrier. On the left side of Fig. 5, single H-evaporation on the ring-closing (C1) dication creates an excited $C_3H_5^{2+}$ (C3) dication at 34.99 eV, where the two end-hydrogen atoms reduce the internal energy by creating a molecular hydrogen and forming the $[CHCHCH]^{2+}$ (C4) dication. The

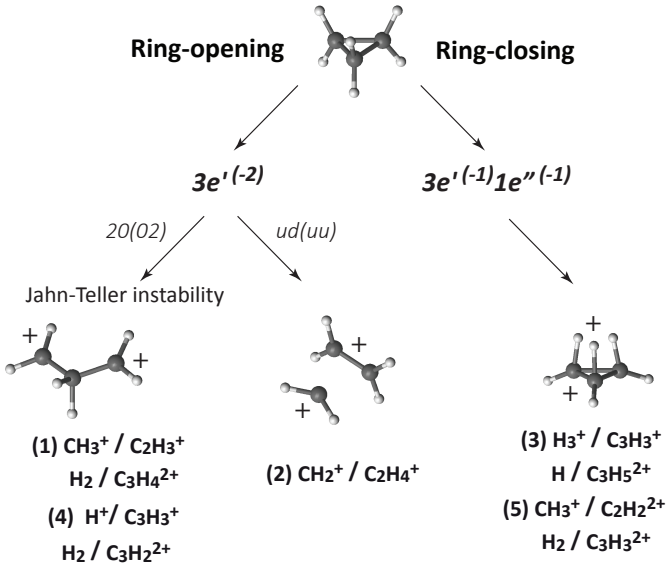

Fig. 6 Cyclopropane dication state-selective dissociation. The $3e'^{-2}$, and $3e'^{-1}\ 1e''^{-1}$ dication states selectively populated by the initially triggered ring-deformation act as a gateway state for the dissociation channels.

Table 2 Experimental values of appearance energy (AE) and kinetic energy released (KER) of the dissociation channels are compared with the calculated values, indicating different amount of internal energy lost.

	AE		KER		
	Exp*	cal	Exp	cal †	$E_{Kautoionization}$
Channel	eV	eV	eV(Γ ∼)	eV	eV
1. $CH_3^+/C_2H_3^+$	29.5 >	27.91‡	5.4(2.0) ≃	5.2 3.70§	1.59
2. $CH_2^+/C_2H_4^+$	31.5 ≃	31.5	5.1(1.5) <	6.54 4.14¶	1.5
3. $H_3^+/C_3H_3^+$	32.5 >	30.31	4.8(1.6)>	3.73	1.13
5. $CH_3^+/C_2H_2^+$	33.0 >	30.91‖	5.2 (1.4)>	3.50	0.39

experimental AE of 35.0 eV for the $C_3H_3^{2+}$ dication in the mass spectrum also agrees well with the minimum reaction pathways. This theoretically explains the H-evaporation pattern observed in the mass spectrum of Fig. 2 (b).

5 Summary and Remarks

We have seen that photochemical reaction in the double ionization continuum of cyclopropane is effectively sensitive to the photon energy. In Table. 2 comparison of the experimental and calculated values of the AE and KER of dissociation channels are shown. Regarding dissociation to the ground state of the fragments, the amount of internal energy lost presented in the last column decreases for the channels appear above the vertical double ionization threshold. We interpreted these values as evidences of sequential double ionization intervening via ring-opening nuclear motion. This is due to the fact that the potential energy of the dication ground state decreases with the extent of ring-opening nuclear motion [see Fig. 4. The larger the extent of ring-opening occurs (on intermediate states) prior to autoionization, the larger the amount of kinetic energy releases through autoionization to the dication ground state. The fact that the initially correlated ring-deformation selectively populate dication states which act as a gateway state of different dissociation channels are presented schematically in Fig. 6. The dissociation channels that involve ring-opening: these reactions are enabled by double ionization of $3e'$ orbitals, on the $3e'^{-2}$ dication state. The dissociation channels that involve ring-closing: these reactions are enabled by ionization of $1e''$ orbitals, on $3e'^{-1}\ 1e''^{-1}$ dication states. The concept of the gateway states can be a subject of a future publication, where the state-selective dissociation is examined in terms of the anti-bonding character of the excited orbitals at the core-to-valence excitation by measuring the branching ratio of the dissociation channels.

∗ Measurements have been done with 0.5 eV step photon energy.
† it is assumed that all the released energy is transferred to kinetic energy of the products.
‡ Related to the dissociation from dication of propene isomer
§ Related to the dissociation to the first electronically excited state of the fragments
¶ Related to the dissociation to the first electronically excited state of the fragments
‖ Related to the dissociation from dication of CH_3CHCH_2 isomer

References

1 R. J. Buenker and S. D. Peyerimhoff, *The Journal of Physical Chemistry*, 1969, **73**, 1299–1313.
2 H. Basch, *The Journal of Chemical Physics*, 1969, **51**, 52.
3 D. Holland, L. Karlsson and K. Siegbahn, *Journal of Electron Spectroscopy and Related Phenomena*, 2002, **125**, 57–68.
4 R. K. Dieter and S. Pounds, *The Journal of Organic Chemistry*, 1982, **47**, 3174–3177.
5 H. Lebel, J.-F. Marcoux, C. Molinaro and A. B. Charette, *Chemical Reviews*, 2003, **103**, 977–1050.
6 H.-U. Reissig and R. Zimmer, *Chemical Reviews*, 2003, **103**, 1151–1196.
7 E. Haselbach, *Chemical Physics Letters*, 1970, **7**, 428–430.
8 J. R. Collins and G. A. Gallup, *J. Am. Chem. Soc.*, 1982, **104**, 1530–1533.
9 K. Ohta, H. Nakatsuji, H. Kubodera and T. Shida, *Chemical Physics*, 1983, **76**, 271–281.
10 T. S. Venkatesan, S. Mahapatra, L. S. Cederbaum and H. KÃűppel, *J. Phys. Chem. A*, 2004, **108**, 2256–2267.
11 G. H. Wannier, *Phys. Rev.*, 1953, **90**, 817–825.
12 T. Balasubramanian, B. N. Jensen, S. Urpelainen, B. Sommarin, U. Johansson, M. Huttula, R. Sankari, E. Nommiste, S. Aksela, H. Aksela, R. Nyholm, R. Garrett, I. Gentle, K. Nugent and S. Wilkins, 2010.
13 S. Urpelainen, M. Huttula, T. Balasubramanian, R. Sankari, P. Kovala, E. Kukk, E. Nommiste, S. Aksela, R. Nyholm, H. Aksela, R. Garrett, I. Gentle, K. Nugent and S. Wilkins, 2010.
14 J. Laksman, D. Céolin, E. P. Månsson, S. L. Sorensen and M. Gisselbrecht, *Rev. Sci. Instrum.*, 2013, **84**, 123113.
15 S. Oghbaie, M. Gisselbrecht, J. Laksman, E. P. Månsson, A. Sankari and S. L. Sorensen, *J. Chem. Phys.*, 2015, **143**, 114309.

16 V. P. Vysotskiy, J. BostrÃűm and V. Veryazov, *J. Comput. Chem.*, 2013, **34**, 2657–2665.

17 P. M. Mayer and L. Radom, *Chemical Physics Letters*, 1997, **280**, 244–250.

18 C. Aubry, M. J. Polce, J. L. Holmes, P. M. Mayer and L. Radom, *J. Am. Chem. Soc.*, 1997, **119**, 9039–9041.

19 P. A. Malmqvist, K. Pierloot, A. R. M. Shahi, C. J. Cramer and L. Gagliardi, *The Journal of Chemical Physics*, 2008, **128**, 204109.

20 F. Aquilante, L. D. Vico, N. Ferrä, G. Ghigo, P. Malmqvist, P. Neogrädy, T. B. Pedersen, M. Pitonìäk, M. Reiher, B. O. Roos, L. Serrano-Andräs, M. Urban, V. Veryazov and R. Lindh, *J. Comput. Chem.*, 2010, **31**, 224–247.

21 D. A. Hagan and J. H. D. Eland, *Org. Mass Spectrom.*, 1992, **27**, 855–863.

22 K. Głuch, J. Fedor, S. Matt-Leubner, O. Echt, A. Stamatovic, M. Probst, P. Scheier and T. D. MaÌĺrk, *The Journal of Chemical Physics*, 2003, **118**, 3090.